Journal of Materials Chemistry A

ROYAL SOCIETY OF CHEMISTRY

PAPER

View Article Online
View Journal | View Issue

Check for updates

Cite this: J. Mater. Chem. A, 2025, 13, 18892

Thermally-induced phase transformations of CALF-20: insights into its phase stability and carbon capture properties†

Dong A. Kang, ‡[a] Navaporn Suphavilai,‡[a] Amro M. O. Mohamed, §[c] Ioannis G. Economou,[c] Manish Shetty,[a] Jinsoo Kim *[d] and Hae-Kwon Jeong *[ab]

Calgary Framework 20 (CALF-20) has garnered a great deal of attention as a promising adsorbent for CO_2 capture applications due to its high CO_2 uptake capacity and excellent stability in humid environments. Multiple studies have explored its adsorption properties and separation performance, while a few studies reveal the existence of several phases of CALF-20, including α-, β-, and τ-phases. α-Phase (*i.e.*, referred as CALF-20) is known to transform into β- or τ-phase under humid or thermal conditions, respectively. Computational studies have shown that β-CALF-20 exhibits a higher heat of CO_2 adsorption, making it more suitable for CO_2 capture compared to α-CALF-20. However, β-CALF-20, transformed from α-CALF-20 under humid conditions, is known to be less stable, thus observed only upon moisture exposure. Here, we demonstrate that β-CALF-20 can be formed solely by thermal treatment of α-CALF-20 and this thermally-derived β-CALF-20 is significantly more stable and can be readily obtained by drying as-synthesized CALF-20 at temperatures above 100 °C. Computational analyses corroborate the experimental results, affirming that the α-to-β phase transformation can be achieved solely through thermal treatment, without the involvement of water, *via* a modification in the Zn coordination number from 5 to 4. More importantly, this study finds that it is challenging to determine gas adsorption properties of α-CALF-20, as degassing of α-CALF-20 at elevated temperatures under vacuum almost always leads to its transformation into β-CALF-20. The resultant β-phase demonstrates a CO_2 uptake of 2.38 mmol g^{-1} at 0.1 bar and 30 °C, along with a CO_2/N_2 IAST selectivity of 222 for a 10 : 90 CO_2/N_2 mixture, which aligns with previous reports. Consequently, these findings imply that previously reported gas adsorption properties, including carbon (CO_2) capture capacities, may have been measured on the β-phase of CALF-20, rather than the α-phase.

Received 3rd March 2025
Accepted 9th May 2025

DOI: 10.1039/d5ta01729g

rsc.li/materials-a

1 Introduction

Carbon capture by physisorption is very promising due to its relatively low regeneration energy and simple operation as compared to other means such as chemisorption and absorption.[1–5] Practical carbon capture by physisorption, however, requires physisorbents exhibiting high specific CO_2 uptake capacity and long-term stability under humid conditions.[6–8] In this regard, the zinc-based Calgary Framework 20 (CALF-20) has recently emerged as a promising physisorbent for CO_2 capture due to its high CO_2 uptake capacity, comparable to high-performance zeolites and other MOFs,[9–13] and, more importantly, its excellent stability in thermal, chemical, and humid environments.[14] This stability arises from the geometric rigidity and strong binding affinity of the 1,2,4-triazolate linker in CALF-20.[9,15,16] Shimizu *et al.*[9] first reported that CALF-20 exhibited a CO_2 capacity of *ca.* 2.6 mmol g^{-1} at 0.10 bar CO_2 and 20 °C, with a CO_2/N_2 IAST (Ideal Adsorbed Solution Theory) selectivity of *ca.* 230 for a 10/90 CO_2/N_2 mixture, comparable to zeolite 13X.[17] However, most CO_2-selective physisorbents including zeolite 13X and MOF-74 suffer from significant loss in CO_2 uptake under humid conditions.[6] In contrast, CALF-20 maintains selective CO_2 adsorption even at 40% relative

[a]*Artie McFerrin Department of Chemical Engineering, Texas A&M University, 3122 TAMU, College Station, TX 77843 3122, USA. E-mail: hjeong7@tamu.edu*

[b]*Department of Materials Science and Engineering, Texas A&M University, 3122 TAMU, College Station, TX 77843 3122, USA*

[c]*Chemical Engineering Program, Texas A&M University at Qatar, PO Box 23874, Doha, Qatar*

[d]*Department of Chemical Engineering (Integrated Engineering), Kyung Hee University, 1732 Deogyeong-daero, Yongin, Gyeonggi-do 17104, Republic of Korea. E-mail: jkim21@khu.ac.kr*

† Electronic supplementary information (ESI) available. See DOI: https://doi.org/10.1039/d5ta01729g

‡ These authors contributed equally to this work.

§ Current address: Qatar Environment and Energy Research Center (QEERI), Hamad Bin Khalifa University, Doha, Qatar.

humidity (RH) owing to its relatively high hydrophobicity compared to other physisorbents.[10,14]

Recently, Farha *et al.*[18] first reported that CALF-20 undergoes a phase transformation upon exposure to humidity. They found that as-dried CALF-20, which they termed α-CALF-20, transformed into β-CALF-20 when exposed to humidity above 23% RH. During the phase transformation, the Zn coordination number decreases from 5 to 4, likely triggered by hydrogen bonding between water molecules and oxalate ligands in the framework. Furthermore, they found that the α-to-β transformation is fully reversible upon exposure of β-CALF-20 to dry air or vacuum. Importantly, their computational studies showed that β-CALF-20 exhibited a higher heat of CO_2 adsorption than α-CALF-20 due to its different pore structure. In β-CALF-20, a CO_2 molecule can interact simultaneously with two oxalate ligands, whereas it can only be in close contact with one ligand in α-CALF-20. This strongly suggests that β-CALF-20 may have a higher CO_2/N_2 selectivity than α-CALF-20. However, they mentioned the β-to-α phase transformation under dry condition made it experimentally challenging to measure the gas adsorption properties of β-CALF-20 since degassing β-CALF-20 would result in its transformation into α-CALF-20.

While we have been independently investigating thermally-induced phase transformation of CALF-20 powders, we have encountered the similar observations made by Janiak *et al.*,[19,20] showing the phase transformations of CALF-20 single crystals upon thermal treatment. After heating α-CALF-20 single crystals at 80 °C for extended periods, they identified two new phases of CALF-20, τ- and γ-phases. Both phases showed an increased Zn coordination number of 6 due to additional coordination with water, compared to 5 in α-CALF-20 and 4 in β-CALF-20.[18] Interestingly, the XRD pattern of τ-CALF-20 single crystals matched that of β-CALF-20 powder sample, despite the difference in their Zn coordination numbers. Both α- and γ-CALF-20 spontaneously transformed into τ-CALF-20 over time, while reversing this transformation proved unsuccessful.[19] This irreversible transformation is in contrast to the reversible α-to-β phase transformation under drying condition as observed by Farha *et al.*,[18] highlighting the need for further clarification of the α-β-τ phase transformation. Moghadam *et al.*[16] also studied phase transformation of CALF-20 upon exposure to humid environments. At 20% RH, CALF-20 underwent the α-to-β transformation similar to that observed by Farha *et al.*[18] When soaked in water, however, CALF-20 experienced different structural changes compared to when exposed to low RH. Their simulations showed that low water loading stabilized a smaller framework volume, while higher humidity (80% RH) caused framework expansion due to water condensation inside the framework. They suggested that hydrophobicity of CALF-20 limited water accommodation, preventing framework expansion at low RH.

In this study, we report that α-CALF-20 can transform into β-CALF-20 by thermal treatment and demonstrate that this thermally-derived β-CALF-20 is more stable than α-CALF-20 and can be readily obtained by drying as-synthesized CALF-20 at temperatures above 100 °C. These findings are supported by *Ab Initio* Molecular Dynamics (AIMD) results, which examine the effects of temperature on the structure of α-CALF-20. We used finite temperature cell AIMD optimization to study the impact of temperature on the local structure of CALF-20. Based on both experimental and computational results, we suggest that previous gas isotherm measurements including carbon capture measurements were likely conducted on β-CALF-20 rather than α-CALF-20, as these measurements were performed after degassing at temperatures above 100 °C under vacuum, which would lead to the formation of β-CALF-20.

2 Experimental section

2.1 Materials

Zinc oxalate dihydrate (99.999%) was purchased from Thermo Fisher Scientific. 1,2,4-Triazole (>98.0%) and methanol (MeOH, >99.8%) were purchased from Sigma Aldrich. All chemicals were used as received without further purification.

2.2 Solvothermal synthesis of CALF-20 powder

CALF-20 powders were synthesized using a solvothermal method as described in the literature.[9,18] A precursor solution was prepared by dissolving 5.00 g of 1,2,4-triazole and 6.60 g of zinc oxalate in 66 ml of methanol in a 125 ml Teflon-lined autoclave. The solution was then transferred to a preheated convection oven and reacted at 180 °C for 2 days. After reaction, the autoclave was allowed to cool to room temperature (RT) naturally. As-synthesized powders were collected by vacuum filtration and washed with 40 ml of methanol. As-washed samples were dried in open-air at RT or preheated ovens with different temperatures for 12 h (80 °C and 150 °C) for further characterization.

2.3 Characterizations

Powder X-ray diffraction (PXRD) patterns were acquired using a Miniflex II X-ray diffractometer from Rigaku, employing Cu-Kα radiation ($\lambda = 1.5406$ Å). Attenuated total reflectance Fourier transform infrared (ATR-FTIR) spectra were obtained using a Nicolet iS5 spectrophotometer (Thermo Scientific) equipped with iD7 ATR with a resolution of 2 cm^{-1} and 50 scans in the wavenumber range of 4000–400 cm^{-1}. Thermogravimetric analysis (TGA) was performed with a Q50 apparatus (TA Instruments) in a temperature range of 25–800 °C with a ramp rate of 5 °C min^{-1} under an air flow rate of 50 cm^3 min^{-1}.

2.4 Gas adsorption measurements

Prior to gas adsorption measurements, the samples were degassed under vacuum at 60 °C for 2 h and then at 100 °C for 12 h following described in the literature.[9] CO_2 and N_2 adsorption isotherms at 30 °C were measured using an ASAP 2020 Plus (Micromeritics) covering an absolute pressure range of 0.0004 to 1 bar. Nitrogen isotherms at 77 K were measured using an Autosorb iQ-C-MP instrument from Anton Paar Quanta Tec. The BET surface areas were estimated from the isotherms at a relative pressure range (p/p_0) of 0.01–0.1, while the micropore volumes were determined by the *t*-plot method at p/p_0 of 0.2–0.5.

2.5 Computational details

In this work, density functional theory (DFT) calculations were used to study the structure of CALF-20. All simulations were performed with the CP2K/QUICKSTEP package,[21] utilizing a plane-wave energy cut-off of 1000 eV and Gamma-point sampling for the Brillouin zone. The interactions between core and valence electrons were modeled using the projector-augmented-wave (PAW) method, while the Perdew–Burke–Ernzerhof (PBE)[22] generalized gradient approximation (GGA) was applied for the exchange-correlation functional. Core electrons were described by Goedecker Teter Hutter (GTH) PBE pseudopotentials,[23,24] and the DZVP-SR-MOLOPT contracted Gaussian basis sets were employed for the optimized Gaussian basis sets (MOLOPT).[25] Within CP2K software, different sets of simulations were performed, either at zero temperature optimization or finite temperature optimization. The final simulation structures output in the form of XRD were analyzed using Mercury software[26] and structural properties were analyzed using the zeo++ code.[27]

We performed *ab initio* molecular dynamics (AIMD) simulations using the CP2K software package. The simulations employed the *NPT*_F ensemble, which maintains constant temperature and pressure while allowing fluctuations in both the shape and volume of the simulation cell. Temperature regulation was achieved using the Canonical Sampling through Velocity Rescaling (CSVR) thermostat. To investigate the cell fluctuations, the system was simulated at 450 K for a total duration of 50 ps, with a time step of 1 fs.

Adsorption properties were computed with Grand Canonical Monte Carlo (GCMC) simulations as implemented in RASPA software.[28] The adsorption isotherms were evaluated by fixing the chemical potential of the adsorbate in the solid phase related to the fugacity of the gas adsorbate at a constant temperature. GCMC simulations were conducted with the assumption of rigid framework and using experimental structures at 303.15 K. A combination of a 12-6 Lennard-Jones (LJ) potential and Coulomb potential was employed to model adsorbate–adsorbate and adsorbate-MOF interactions. The partial atomic charges of the framework atoms were generated *via* PACMOF.[29] The LJ parameters for the framework were derived from DREIDING force field.[30] For CO_2 molecules, force field developed by Garcia-Sanchez *et al.*[31] was utilized as other studies in CALF-20 structure. The Lorentz–Berthelot mixing rules were used to calculate interactions between dissimilar species. The LJ potential was truncated at a cutoff distance of 12.8 Å, and tail corrections were applied. Long-range electrostatic interactions were computed using the Ewald summation method. MC moves were implemented such as insertion/deletion, translation, rotation and reinsertion. The simulations ran for a total of 100 000 initialization cycles and 100 000 production cycles.[28]

3 Results and discussion

Fig. 1 presents the PXRD patterns of as-synthesized CALF-20 powders (*i.e.*, powders obtained immediately after vacuum filtration and methanol washing), dried under various conditions, alongside the simulated patterns of different CALF-20 phases. The phase of each CALF-20 sample was assigned based on the simulated patterns.[9,18] The simulated pattern by Shimizu *et al.*[9] corresponds to CALF-20 single crystals (termed α′-phase) containing ethanol molecules (see Fig. S1†). Later, Farha *et al.*[18] identified two distinct phases of CALF-20 powders, α- and β-phases, which do not contain solvent molecules. They found that β-CALF-20 form when α-CALF-20 powders are exposed to humid conditions. While we were preparing this manuscript, it came to our attention that Janiak *et al.*[19] reported τ-CALF-20 single crystals, obtained by heating α′-CALF-20 single crystals at 80 °C for 7 days, with an XRD pattern similar to that of β-CALF-20 powders reported by Farha *et al.*[18] (see Fig. S2†). Fig. S1† presents the crystal structures of these phases along with unit cell information. It is important to note the differences in the synthesis conditions for β- and τ-CALF-20: Farha *et al.*[18] investigated CALF-20 powders synthesized using zinc oxalate dihydrate as the metal precursor and pure methanol as the solvent, while Janiak *et al.*[19] studied α′-CALF-20 single crystals synthesized using zinc nitrate hexahydrate and 50% ethanol, following the same method as Shimizu *et al.*[9] It is worthy of mentioning here that this difference in the synthesis conditions has a significant implication, in that while Farha's α-CALF-20 powders do not contain much water (mostly methanol), Janiak's α′-CALF-20 single crystals contain water molecules as well as ethanol inside. In this work, we focus on CALF-20 powders synthesized using the synthesis condition by Farha *et al.*[18] to examine phase behaviors of CALF-20 from a practical

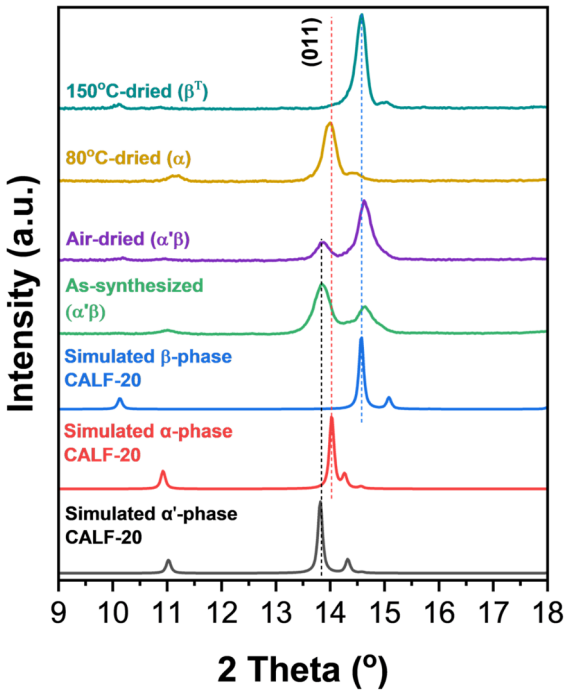

Fig. 1 PXRD patterns of CALF-20 powders after treatment of as-synthesized CALF-20 powders (mixed phase) under different drying conditions in comparison with simulated patterns of α′-, α-, and β-CALF-20.

perspective. For clarity, we designate the phase obtained by thermal treatment of α-CALF-20 powders as 'β^T' to differentiate it from both β-CALF-20 and τ-CALF-20, which result from exposing α-CALF-20 powders to humid conditions and from thermally treating α′-CALF-20 single crystals, respectively. It is noted that the CALF-20 single crystal synthesized in ethanol[9] is referred to as α′-CALF-20 in this study to distinguish it from the α-CALF-20 phase (*i.e.*, as-activated CALF-20 powders) reported by Farha *et al.*[18](see Fig. S1†).

As shown in Fig. 1, both the as-synthesized and air-dried CALF-20 powders exhibit mixed phases (α′– and β-phases). We found it quite challenging to obtain phase-pure CALF-20. Nevertheless, based on the intensity of the (011) plane, when dried in an ambient condition (*i.e.*, air-dried), the sample contains a higher proportion of the β-phase than the as-synthesized sample likely due to the adsorption of atmospheric moisture, favoring the formation of the β-phase. Sun *et al.*[32] made a similar observation, where atmospheric drying at room temperature for 12 h led to the formation of mixed α′- and β-phases.

When the as-synthesized CALF-20 powders (mixed phases) were dried in a preheated oven at different temperatures, the resulting XRD patterns revealed distinct phases: (1) α-phase after drying at 80 °C for 12 h and (2) β-phase after drying at 150 °C for 12 h (hereafter, β^T-phase). This thermally-induced phase formation of α-phase to β^T-phase was unexpected as Farha *et al.*[18] reported that β-phase of CALF-20 powders formed when α-CALF-20 powders were exposed to water vapor. As mentioned above, however, after seeing the report by Janiak *et al.*,[19] we realized that this thermally-induced phase formation of α-phase to β^T-phase could be possible due to the flexibility of the CALF-20 framework.

Interestingly, β^T-CALF-20 powders exhibits an XRD pattern similar to τ-CALF-20 reported by Janiak *et al.*[19] (Fig. S2†). It is reminded that τ-CALF-20 contained considerable amount of water and formed due to an additional coordination of the zinc centers with water molecules when α-CALF-20 single crystals (hereafter, α′-CALF-20) were treated at 80 °C for 7 days.[19] In contrast, β^T-CALF-20 formed from thermal treatment of α-CALF-20 powders at temperatures much higher (*i.e.*, 150 °C) than the thermal conditions employed by Janiak *et al.*[19] It is, therefore, surmised that our β^T-phase is not likely to contain substantial amount of water, distinctively different from τ-CALF-20. Additionally, the PXRD patterns presented in Fig. 1 were performed immediately after removing the samples from the oven, and the scans were conducted quickly (within *ca.* 3 min) to minimize any effects of atmospheric moisture in the X-ray chamber. The PXRD patterns of both α- and β-CALF-20, covering a broader 2θ range and obtained with a typical X-ray scan rate, are available in Fig. S3.† The observations made above strongly suggest that (1) β-phase can be obtained *via* thermal treatment (*i.e.*, β^T-phase), not only *via* moisture treatment by Farha *et al.*[18] but also that (2) β^T-phase is not likely the same as τ-phase reported by Janiak *et al.*[19] since formation of τ-phase is possible only with water molecules inside its framework which is unlikely in the case of β^T-phase (*vide infra*).

We attempted to confirm the α-to-β transformation upon exposure to moisture as reported by Farha *et al.*[18] The α-CALF-20 powders were obtained by drying as-synthesized CALF-20 at 80 °C and exposed to a closed humid chamber (77% RH) containing a saturated NaCl aqueous solution (see Fig. S4†) at room temperature. As shown in Fig. S5,† exposure to 77% RH for 1 to 3 h resulted in mixed phases of CALF-20 with the (011) peak of β-CALF-20 intensifying over time. The sample was fully transformed to β-CALF-20 after 1 day of moisture exposure, consistent with the findings of Farha *et al.*[18] After prolonged exposure (*i.e.*, 3 days), however, the sample reverted to the α′-phase of CALF-20. Recently, Moghadam *et al.*[16] reported similar results, noting that when exposure to 20% RH and soaking in water, the XRD patterns of CALF-20 showed β-phase and α′-phase, respectively, judging from the (011) peak. The formation of α′-phase was attributed to the expansion of the CALF-20 framework caused by water condensation within the framework,[16] confirming the flexibility of CALF-20 framework.

To evaluate the stability of the α- and β^T-phases obtained by drying as-synthesized samples at 80 °C and 150 °C, respectively, both CALF-20 samples were exposed to open air, and their PXRD patterns were monitored over time. As shown in Fig. S6a,† the α-phase (obtained by drying at 80 °C) underwent a clear phase transformation into a mixture of α′– and β-phases likely due to atmospheric moisture. This transformation stabilized after 5 days of exposure. In contrast, the β^T-CALF-20 (obtained by drying at 150 °C) showed no phase transformation even after 10 days of exposure (Fig. S6b†). These results suggest that α-phase is relatively less stable than β^T-phase under atmospheric conditions. Janiak *et al.*[19] made similar observation in that α-phase was not as stable based on the fact that α-CALF-20 single crystals (*i.e.*, α′-phase) spontaneously transformed into τ-CALF-20 single crystals over time. Notably, this α′-to-τ-phase transformation turned out irreversable.[19]

Fig. 2a shows the FTIR spectra of CALF-20 samples treated under different drying conditions. Like the PXRD measurements, all FTIR measurements were conducted immediately after removing the samples from the oven to minimize atmospheric moisture effects. The spectra for all samples display characteristic bands corresponding to the functional groups of CALF-20. Notable differences are observed around the wavenumber *ca.* 3400 cm^{-1}, corresponding to O–H bond stretching. The as-synthesized sample exhibits the strongest O–H stretching peak, more likely due to residual methanol than to water within the CALF-20 framework. After air drying for 12 h, although the O–H absorbance decreases significantly, the absorbance remains, possibly due to residual methanol and adsorbed atmospheric water molecules. In contrast, both α- and β^T-CALF-20 samples, obtained by drying at 80 °C and 150 °C, respectively, show no distinct broad O–H band in this region, confirming the effective removal of methanol (and water) in these samples. This proves that unlike τ-CALF-20, our β^T-CALF-20 has neither residual methanol nor water molecules coordinated with the zinc centers.

Fig. S7† presents the TGA curves of α- and β^T-CALF-20 powders. Both samples exhibit weight loss below *ca.* 100 °C and 60 °C, respectively, due to the removal of guest molecules

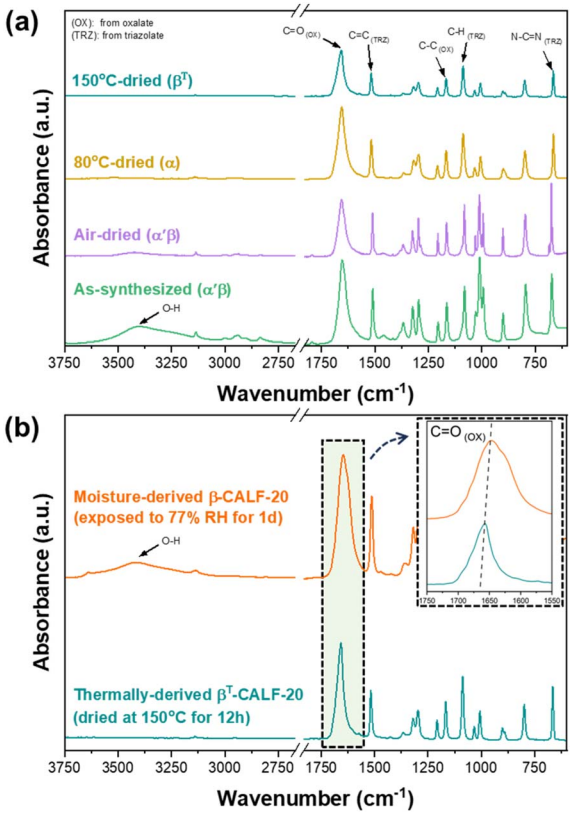

Fig. 2 Fourier transform infrared (FTIR) spectra of CALF-20: (a) treated under different drying conditions and (b) comparison between thermally-derived β^T-CALF-20 *vs.* moisture-derived β-CALF-20.

(*i.e.*, methanol and/or water). Notably, α-CALF-20 shows a higher weight loss (*ca.* 7.2 wt%) compared to β^T-CALF-20 (*ca.* 4.9 wt%). This difference stems likely from the possible presence of residual methanol in α-CALF-20. On the other hands, β^T-CALF-20 treated at 150 °C is expected to contain no residual methanol. The weight loss below *ca.* 60 °C is likely due to adsorbed water during the sample preparation and TGA measurement. It is worth noting here that γ-CALF-20 reported by Janiak *et al.*,[19] obtained by heating α-CALF-20 single crystals at 80 °C for 10 days, showed a higher weight loss (*ca.* 11 wt%) due to the removal of guest molecules (both ethanol and water) than our β^T-CALF-20 powders. Although TGA data on τ-CALF-20 was not provided in their report,[19] it is speculated that τ-CALF-20 single crystals contained more water molecules than γ-CALF-20 single crystals since they were treated at the same temperature but for shorter time (7 days *vs.* 10 days).

Fig. 2b compares the FTIR spectra of two β-CALF-20 samples, thermally-derived (β^T) and moisture-derived (β). Unlike the thermally-derived β^T-CALF-20 powders (dried at 150 °C), the moisture-derived β-CALF-20 (exposed to 77% RH) shows notable O–H peak at *ca.* 3400 cm^{-1}. It is noted that both β-CALF-20 powders and τ-CALF-20 single crystals reported by Farha *et al.*[18] and Janiak *et al.*,[19] respectively, exhibited distinct O–H peaks in their FTIR spectra. This suggests that, unlike previous reports,[18,19] β-CALF-20 (or τ-CALF-20) can be stabilized without water molecules coordinated to the framework. Furthermore, there is a blue shift of the C=O bands of oxalate groups in the thermally-derived β^T-CALF-20 as compared to the moisture-derived β-CALF-20, indicating stronger interaction of oxalate groups and zinc centers in β^T-CALF-20. It is noted that the C=O bands of α- and β^T-CALF-20 show no significant differences in terms of peak position and broadening (see Fig. 2a). These observations indicate that the formation of β^T-phase does not necessarily involve interactions between the C=O bonds of oxalate groups and water molecules as in the case of β-phase formation proposed by Farha *et al.*[18]

The observed irreversible α-to-β^T transformation at higher temperatures implies that the β-phase represents a lower-energy state at elevated temperatures, as additional thermal energy likely facilitates overcoming activation barriers between the phases. Furthermore, the reduced cell volume of β-phase compared to α-phase (Fig. S1†) indicates a denser packing of the framework.[33] This increased density may enhance energetic stability by minimizing free space within the structure.

Fig. 3a presents the PXRD patterns of CALF-20 samples after degassing prior to isotherm measurement and after CO_2 isotherm measurement in comparison with that of as-synthesized powders. The adsorption measurements were conducted on as-synthesized CALF-20 powders after degassing at 60 °C for 2 h and subsequently at 100 °C for 12 h under vacuum, following a protocol by Shimizu *et al.*[9] Consistent with the above observations, the PXRD pattern after thermal degassing under vacuum confirms the transformation of mixed-phase to β^T-phase. The BET surface area and micropore volume were estimated to be *ca.* 531 $m^2\ g^{-1}$ and 0.207 cm^3, respectively, based on the N_2 adsorption isotherm at 77 K (Fig. S8a†). These values align well with those reported in the literature (Table S1†).[9,13,16,18] Fig. S8b† presents the CO_2 and N_2 adsorption isotherms at 30 °C. The sample exhibited a CO_2 uptake capacity of *ca.* 2.38 mmol g^{-1} at 0.1 bar and a CO_2/N_2 IAST selectivity of *ca.* 222 for a 10 : 90 CO_2/N_2 mixture. These results are consistent with previously reported values on CALF-20 (Table S1†). β^T-phase remained stable even after the CO_2 isotherm measurements (Fig. 3a). Notably, our repeated attempts to obtain activated α-CALF-20 samples after degassing under various conditions proved unsuccessful. This is because extensive degassing of α-CALF-20 powders, required for precise isotherm measurements, invariably resulted in the formation of β^T-CALF-20. Fig. 3b compares the experimental CO_2 isotherm of our β^T-CALF-20 and that of CALF-20 reported by Shimizu *et al.*,[9] showing only minor differences. This observation suggests that the gas adsorption properties of CALF-20, such as carbon capture, previously reported in the literature might be based on β^T-CALF-20 rather than α-CALF-20.

To computationally investigate the structural behavior of CALF-20 in the absence of solvents, Density Functional Theory (DFT) and Molecular Dynamics (MD) simulations were employed to optimize the framework at finite temperatures. MD simulations in the NVT ensemble were conducted over a temperature range of 300–700 K to examine changes in Zn coordination. At 300 K and 450 K, the Zn coordination number of 4 was observed, consistent with the β-CALF-20 phase, while α-CALF-20 has the coordination number of 5, as reported by Farha

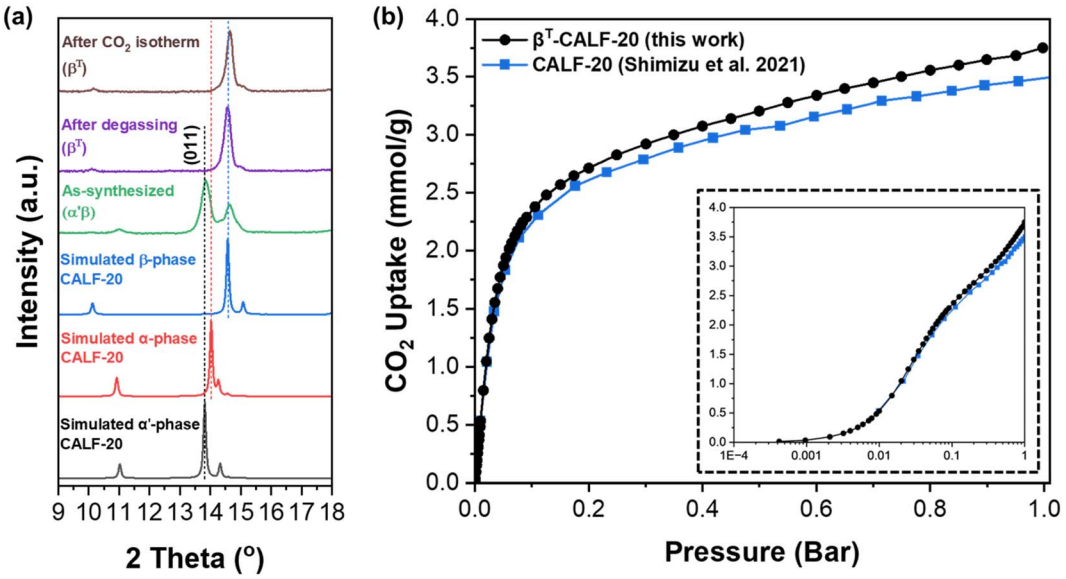

Fig. 3 (a) PXRD patterns of CALF-20 after degassing and after CO_2 isotherm measurement in comparison with that of as-synthesized powders along with simulated patterns and (b) CO_2 isotherm of our β^T-CALF-20 in comparison with that of CALF-20 reported by Shimizu *et al.*[4] (inset: a semi-log plot).

et al.[18] As the temperature increased, CALF-20 was transformed from α-CALF-20 to β-CALF-20 in terms of Zn coordination, suggesting that temperature-induced transformations under vacuum conditions might stabilize the β-phase. However, no discernible shifts in XRD peaks were observed during these simulations, highlighting the need for further investigation.

Additionally, AIMD simulations in the *NPT* ensemble were performed at 450 K over 50 ps with a time step of 1 fs. Starting from the α-CALF-20 structure, changes in Zn coordination (Fig. S9†) and new peaks in the XRD pattern (Fig. 4a) were observed. A comparison of AIMD snapshots with DFT-optimized structures of α- and β-phases revealed that structural fluctuations resulted in β-CALF-20 phase characteristics in the simulated XRD patterns. These findings suggest that CALF-20 undergoes phase fluctuations at elevated temperatures, with cell volumes oscillating between 697.7 $Å^3$ and 767.7 $Å^3$. This study indicates that α-CALF-20 can transform into β-CALF-20 through thermal stimulation alone, driven by changes in Zn coordination, without the involvement of water, which contrasts the reports by Farha *et al.*[18] and Janiak *et al.*[19] These simulation results align with our experimental observations, where β-CALF-20 (*i.e.*, β^T-CALF-20) was obtained by heating α-CALF-20 at 150 °C for 12 h.

Atomistic GCMC simulations were performed to predict the CO_2 adsorption capacities of both α- and β-CALF-20. Structural models from previous studies by Shimizu *et al.*[9] and Farha *et al.*[18] were used for the computations. The results show that the CO_2 adsorption capacities of α- and β-CALF-20 are comparable at 1 bar and 30 °C (Fig. 4b). Notably, the calculated CO_2 capacity of τ-CALF-20 (*ca.* 2.5 mmol g^{-1} at 1 bar and 25 °C) reported by Janiak *et al.*,[19] which exhibits an XRD pattern similar to that of β-CALF-20, was significantly lower than that of CALF-20 (*ca.* 4 mmol g^{-1} at 1 bar and 25 °C) reported by Shimizu *et al.*[9] This supports the hypothesis that earlier experimental adsorption measurements in reports were likely conducted on β-CALF-20 rather than α-CALF-20, as previously discussed. While the adsorption properties of the two phases are similar, differences in their diffusion behaviors are expected due to the twisting of oxalate linkers and the more compact porous structure of β-CALF-20. These structural differences could significantly influence the kinetics of gas transport, a factor not explicitly addressed in this study. However, a preliminary investigation into diffusion behavior has been reported previously.[18] To fully elucidate the impact of these structural variations on gas separation performance, future work should focus on comprehensive studies of diffusion coefficients and transport properties.

Integrating the findings from Farha *et al.*[18] and Janiak *et al.*[19] with our results, we propose that the α-to-β phase transformation in CALF-20 is driven by a change in Zn coordination number from 5 to 4, which can be induced by either moisture or thermal effects. It is plausible that the τ-CALF-20 phase, exhibiting a similar XRD pattern to β-CALF-20 as reported by Janiak *et al.*,[19] was influenced by both moisture and thermal factors. Their drying process for α-CALF-20 at 80 °C over 7 days may not have been sufficient to completely remove water molecules from the framework. This incomplete removal could have permitted water to coordinate with the CALF-20 structure along with the formation of thermally-derived stable β-CALF-20, potentially leading to the lower CO_2 uptake predicted by simulation for τ-CALF-20 compared to α- and β-CALF-20.[19]

Experimental observations from both our study and Janiak *et al.*[19] indicate that β-CALF-20 (or τ-CALF-20) is more stable than α-CALF-20 and cannot revert to the α-phase. In contrast, Farha *et al.*[18] reported that moisture-derived β-CALF-20 could be transformed back to α-CALF-20 upon the removal of water from

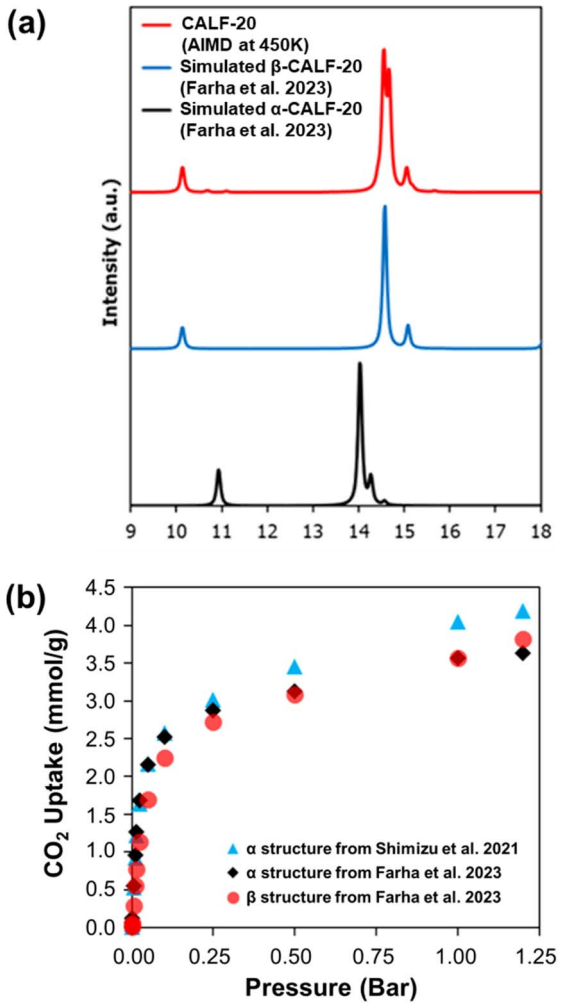

Fig. 4 (a) XRD patterns of CALF-20 under thermal variations obtained through AIMD simulation at 450 K and 1 bar, alongside reference simulated patterns of α- and β-CALF-20 adapted from Farha *et al.*[13] and (b) CO_2 isotherms at 30 °C of literature α and β-CALF-20 structures using GCMC simulations performed in this work.

the framework. Farha *et al.*[18] hypothesized that the α-to-β transformation arises from hydrogen bonding between water and oxalate groups, which alters Zn coordination from 5 to 4. On the other hand, Janiak *et al.*[19] suggested that the transformation involves additional coordination of Zn with water, increasing the coordination number to 6. These differing interpretations, combined with our findings, highlight the complexity of the α-to-β phase transformation and underscore the need for further investigation to elucidate the precise mechanisms. Revisiting these phenomena may provide valuable insights into the interplay of thermal and moisture effects on the CALF-20 framework, which eventually affect the carbon capture properties of the framework and their performance under high humidity.

4 Conclusions

In this study, we examined the phase transformation and stability of CALF-20 under various environmental conditions, including atmospheric, humid, and thermal conditions. While the moisture-induced α-to-β phase transformation of CALF-20 has been reported previously, our findings demonstrate that this transformation can also be achieved through thermal treatment. Specifically, β-CALF-20 (*i.e.*, β^T-CALF-20) was consistently obtained by drying or degassing as-synthesized powders at temperatures exceeding 100 °C. We observed that α-CALF-20 was relatively unstable, undergoing phase changes even under mild conditions such as atmospheric exposure at room temperature, resulting in mixed phase. In contrast, the thermally-derived β^T-CALF-20 exhibited remarkable stability under similar conditions. Our molecular simulations support these experimental observations, showing that thermal treatment of α-CALF-20 in a solvent-free environment induces localized and structural modifications, leading to the formation of β^T-CALF-20. Notably, the gas adsorption properties of β^T-CALF-20 observed in this study closely resemble those reported in prior studies.[9,13,18] While direct comparisons are limited, this similarity suggests that previous measurements of gas adsorption isotherms of CALF-20, particularly for carbon capture, may have been conducted on the β^T-phase, possibly formed inadvertently during sample activation or processing. These findings underscore the importance of clearly identifying and reporting the structural phase of CALF-20 when evaluating and comparing material properties across studies.

Data availability

Data supporting this study are included within the article and/or ESI.†

Conflicts of interest

There are no conflicts to declare.

Acknowledgements

H.-K. J. acknowledges financial support from the Korea Evaluation Institute of Industrial Technology (KEIT) funded by the Ministry of Trade, Industry & Energy (MOTIE, Korea) (Project: 20018346). This work was supported in part by Brain Pool Program through the National Research Foundation of Korea (NRF) funded by the Ministry of Science and ICT (RS-2024-00400935). The authors would like to thank Dr Abdoulaye Djire, Mr Ray Yoo and Ms. Jenna Vito at Texas A&M University for their assistance in obtaining N_2 porosimetries of MOFs samples. The authors are thankful of Mr Andres Ramos at Texas A&M University for his experimental assistance. We are grateful to the High-Performance Computing Center of Texas A&M University at Qatar for its generous resource allocation.

Notes and references

1 C.-H. Yu, C.-H. Huang and C.-S. Tan, *Aerosol Air Qual. Res.*, 2012, **12**, 745–769.
2 P. Madejski, K. Chmiel, N. Subramanian and T. Kuś, *Energies*, 2022, **15**, 887.

3 W. L. Li, Q. Shuai and J. Yu, *Small*, 2024, **20**, 2402783.
4 X. Y. D. Soo, J. J. C. Lee, W.-Y. Wu, L. Tao, C. Wang, Q. Zhu and J. Bu, *J. CO_2 Util.*, 2024, **81**, 102727.
5 Y. Tao and H. Xu, *Appl. Therm. Eng.*, 2024, **236**, 121504.
6 N. C. Burtch, H. Jasuja and K. S. Walton, *Chem. Rev.*, 2014, **114**, 10575–10612.
7 A. Kumar, D. G. Madden, M. Lusi, K. J. Chen, E. A. Daniels, T. Curtin, J. J. Perry IV and M. J. Zaworotko, *Angew. Chem., Int. Ed.*, 2015, **54**, 14372–14377.
8 M. Khraisheh, S. Mukherjee, A. Kumar, F. Al Momani, G. Walker and M. J. Zaworotko, *J. Environ. Manage.*, 2020, **255**, 109874.
9 J.-B. Lin, T. T. Nguyen, R. Vaidhyanathan, J. Burner, J. M. Taylor, H. Durekova, F. Akhtar, R. K. Mah, O. Ghaffari-Nik, S. Marx, N. Fylstra, S. S. Iremonger, K. W. Dawson, P. Sarkar, P. Hovington, A. Rajendran, T. K. Woo and G. K. H. Shimizu, *Science*, 2021, **374**, 1464–1469.
10 T. T. Nguyen, J.-B. Lin, G. K. Shimizu and A. Rajendran, *Chem. Eng. J.*, 2022, **442**, 136263.
11 Y. Magnin, E. Dirand, G. Maurin and P. L. Llewellyn, *ACS Appl. Nano Mater.*, 2023, **6**, 19963–19971.
12 T. T. Nguyen, G. K. Shimizu and A. Rajendran, *Chem. Eng. J.*, 2023, **452**, 139550.
13 Y. Higuchi, M. Sugita, S. Moriya, T. Takewaki and S. Tanaka, *Microporous Mesoporous Mater.*, 2024, **374**, 113137.
14 A. Rajendran, G. K. Shimizu and T. K. Woo, *Adv. Mater.*, 2024, **36**, 2301730.
15 Z. Shi, Y. Tao, J. Wu, C. Zhang, H. He, L. Long, Y. Lee, T. Li and Y.-B. Zhang, *J. Am. Chem. Soc.*, 2020, **142**, 2750–2754.
16 R. Oktavian, R. Goeminne, L. T. Glasby, P. Song, R. Huynh, O. T. Qazvini, O. Ghaffari-Nik, N. Masoumifard, J. L. Cordiner, P. Hovington, V. Van Speybroeck and P. Z. Moghadam, *Nat. Commun.*, 2024, **15**, 3898.
17 P. Nugent, Y. Belmabkhout, S. D. Burd, A. J. Cairns, R. Luebke, K. Forrest, T. Pham, S. Ma, B. Space and L. Wojtas, *Nature*, 2013, **495**, 80–84.
18 Z. Chen, C.-H. Ho, X. Wang, S. M. Vornholt, T. M. Rayder, T. Islamoglu, O. K. Farha, F. Paesani and K. W. Chapman, *ACS Mater. Lett.*, 2023, **5**, 2942–2947.
19 J. Drweska, F. Formalik, K. Roztocki, R. Q. Snurr, L. J. Barbour and A. M. Janiak, *Inorg. Chem.*, 2024, **63**, 19277–19286.
20 J. Drwęska, K. Roztocki and A. M. Janiak, *Chem. Commun.*, 2025, **61**, 1032–1047.
21 J. Hutter, M. Iannuzzi, F. Schiffmann and J. VandeVondele, *Wiley Interdiscip. Rev.: Comput. Mol. Sci.*, 2014, **4**, 15–25.
22 J. P. Perdew, K. Burke and M. Ernzerhof, *Phys. Rev. Lett.*, 1996, **77**, 3865.
23 S. Goedecker, M. Teter and J. Hutter, *Phys. Rev. B:Condens. Matter Mater. Phys.*, 1996, **54**, 1703.
24 C. Hartwigsen, S. Gœdecker and J. Hutter, *Phys. Rev. B:Condens. Matter Mater. Phys.*, 1998, **58**, 3641.
25 J. VandeVondele and J. Hutter, *J. Chem. Phys.*, 2007, **127**, 114105.
26 C. F. Macrae, I. Sovago, S. J. Cottrell, P. T. Galek, P. McCabe, E. Pidcock, M. Platings, G. P. Shields, J. S. Stevens and M. Towler, *Appl. Crystallogr.*, 2020, **53**, 226–235.
27 T. F. Willems, C. H. Rycroft, M. Kazi, J. C. Meza and M. Haranczyk, *Microporous Mesoporous Mater.*, 2012, **149**, 134–141.
28 D. Dubbeldam, S. Calero, D. E. Ellis and R. Q. Snurr, *Mol. Simul.*, 2016, **42**, 81–101.
29 S. Kancharlapalli, A. Gopalan, M. Haranczyk and R. Q. Snurr, *J. Chem. Theory Comput.*, 2021, **17**, 3052–3064.
30 S. L. Mayo, B. D. Olafson and W. A. Goddard, *J. Chem. Phys.*, 1990, **94**, 8897–8909.
31 A. Garcia-Sanchez, C. O. Ania, J. B. Parra, D. Dubbeldam, T. J. Vlugt, R. Krishna and S. Calero, *J. Phys. Chem. C*, 2009, **113**, 8814–8820.
32 Y. Wei, F. Qi, Y. Li, X. Min, Q. Wang, J. Hu and T. Sun, *RSC Adv.*, 2022, **12**, 18224–18231.
33 J. Nyman and G. M. Day, *CrystEngComm*, 2015, **17**, 5154–5165.